Liquid Crystals
Publication details, including instructions for authors and subscription information:
http://www.informaworld.com/smpp/title~content=t713926090

Dynamic and microscopic X-ray characterization of a compound chevron layer in electroclinic liquid crystals

Atsuo Iida[a]; Yumiko Takahashi[b]; Yoichi Takanishi[c]; Michi Nakata[c]; Ken Ishikawa[c]; Hideo Takezoe[c]
[a] Photon Factory, Institute of Materials Structure Science, High Energy Accelerator Research Organization, 1-1 Oho Tsukuba, Ibaraki 305-0801, Japan [b] Department of Physics, Nihon University, Surugadai, Kanda, Chiyoda-ku, Tokyo 101-8308, Japan [c] Department of Organic and Polymeric Materials, Tokyo Institute of Technology, O-okayama, Meguro-ku, Tokyo 152-8552, Japan

To cite this Article Iida, Atsuo , Takahashi, Yumiko , Takanishi, Yoichi , Nakata, Michi , Ishikawa, Ken and Takezoe, Hideo(2005) 'Dynamic and microscopic X-ray characterization of a compound chevron layer in electroclinic liquid crystals', Liquid Crystals, 32: 6, 717 — 726
To link to this Article: DOI: 10.1080/02678290500117704
URL: http://dx.doi.org/10.1080/02678290500117704

Liquid Crystals, Vol. 32, No. 6, June 2005, 717–726

Taylor & Francis
Taylor & Francis Group

Dynamic and microscopic X-ray characterization of a compound chevron layer in electroclinic liquid crystals

ATSUO IIDA*†, YUMIKO TAKAHASHI‡, YOICHI TAKANISHI§, MICHI NAKATA§, KEN ISHIKAWA§ and HIDEO TAKEZOE§

†Photon Factory, Institute of Materials Structure Science, High Energy Accelerator Research Organization, 1-1 Oho Tsukuba, Ibaraki 305-0801, Japan

‡Department of Physics, Nihon University, Surugadai, Kanda, Chiyoda-ku, Tokyo 101-8308, Japan

§Department of Organic and Polymeric Materials, Tokyo Institute of Technology, O-okayama, Meguro-ku, Tokyo 152-8552, Japan

(*Received 17 January 2005; accepted 10 February 2005*)

The local layer structure of surface stabilized electroclinic liquid crystals has been analysed by time-resolved synchrotron X-ray microdiffraction. At a low applied electric field, the initial bookshelf structure starts to respond above a threshold voltage. With a low to medium applied field of triangular form, the layer structure transforms reversibly between the bookshelf (low field) and the compound chevron (high field), in which the vertical and horizontal chevrons alternate along the layer. When the horizontal chevron component appears, a stripe texture can be seen in an optical micrograph. With increasing field, the horizontal chevron becomes a dominant structure while the vertical chevron still remains. The layer spacing changes in correlation with the chevron angle during the field application. At high field, surface molecules partly rearrange, resulting in alignment deterioration at the interface. The layer response time for an a.c. square wave field is of the order of a few μs to ten μs, which is close to the optical response. The appearance of the compound chevron is discussed in conjunction with the anchoring effect.

1. Introduction

The electroclinic effect [1] has attracted much attention as a pre-transition phenomenon in the chiral smectic A (SmA) phase near the SmA–smectic C* (SmC*) phase transition, and also as a potential candidate for electro-optic applications. Many studies have been performed for analysis of the molecular response in the electroclinic effect [2–6]. With the application of an electric field along the layer, SmA molecules tilt in a plane perpendicular to the applied field. To understand the electro-optical behaviour, it is also important to know the dynamic layer structure under the effect of the electric field. The constriction of layer spacing due to the molecular tilt during the electroclinic effect is expected to generate a buckling of the initial bookshelf layer structure. Although the vertical chevron structure (v-chevron) in the SmC* phase is a well established layer structure due to layer shrinkage [7], the layer structure in the electroclinic effect has not been fully clarified. It is also noted that a stripe texture along the rubbing direction often appears in the electroclinic effect when viewed with a polarizing optical microscope [5, 6]. A similar stripe texture appears also in the SmC* and SmC_A* phases under a high electric field [8] or without an electric field [9]. Johno *et al*. [10] observed side peaks in X-ray small angle scattering profiles from electroclinic liquid crystals, indicating the appearance of the partial v-chevron. Later, the v-chevron in the electroclinic effect was also observed by X-ray study [11]. On the other hand, the horizontal chevron (h-chevron, in-plane chevron) was clearly confirmed for other materials having a relatively large induced tilt angle [12–14]. A light-scattering experiment also suggested a strong correlation between stripe texture and the h-chevron [15]. Based on these results, theoretical treatments of the layer structure in the electroclinic effect have been developed for the h-chevron [5, 16–18] and v-chevron [19]. Since most observations have been performed on a macroscopic scale, except for the spatially resolved optical experiment [20], the local layer structure in the electroclinic effect has not yet been directly analysed.

Recent studies on the ferroelectric, ferrielectric and antiferroelectric phases [21–24] have raised a wide

*Corresponding author. Email: atsuo.iida@kek.jp

Liquid Crystals
ISSN 0267-8292 print/ISSN 1366-5855 online © 2005 Taylor & Francis Group Ltd
http://www.tandf.co.uk/journals
DOI: 10.1080/02678290500117704

interest in the various types of layer structure in relation to the stripe texture. Time-resolved synchrotron X-ray microdiffraction, with a few μm spatial resolution and a few μs time resolution, has been applied to the analysis of the local layer structure in these modulated textures [25, 26]. In this paper, the static and dynamic local layer structures in the electroclinic effect are analysed by this time resolved X-ray microdiffraction. The static and transient layer responses to the triangular and step wave-form electric fields, respectively, are measured. The local layer structure is discussed, as well as the relationship between the layer response and the molecular orientation.

2. Experimental

The ferroelectric liquid crystal sample was TK-C101 (Chisso) [27] sandwiched between ITO-coated glass plates (80 μm thick) with polyimide alignment films. The phase sequence of TK-C101 is isotropic (80°C) N* (70°C) SmA (56°C) SmC*. The experiments were performed in the SmA phase at 0.5–1.0°C above T_c, where T_c is the phase transition temperature from SmA to SmC*. Most of the experiments were carried out with one-side rubbing cells, although a both-sides rubbing cell and a cell without rubbing treatment were also used for comparison. The sample and cell alignment conditions were almost the same as in previous experiments [25, 26]. The cell gap was about 5–8 μm.

The experimental conditions are briefly presented here; for details see [25]. The synchrotron X-ray diffraction experiments were carried out on beam-line 4A at the Photon Factory. The incident X-ray energy was 8 keV (1.55 Å). The beam size was about $3(\mathrm{h}) \times 4(\mathrm{v})\,\mu\mathrm{m}^2$ and the angular divergence of the incident beam was about 1.0 mrad both in the horizontal and in the vertical directions. The rubbing direction was set horizontally. The layer deflection angles, δ and γ, are defined in figure 1. The χ intensity distribution (χ-profile) was recorded on a position-sensitive proportional counter (PSPC), while the ω-scan intensity profile (ω-profile) was obtained by rotating the sample around a vertical axis (Y). The ω intensity is the integrated intensity with respect to χ. The time-resolved ω-profile and χ-profile were obtained with a multi-channel scaler (MCS) mode and a gated multichannel analyser (MCA) mode, respectively. MCS and MCA data were summed within a measurement time. The layer spacing measurement was made with an X-ray image-intensified CCD (II CCD) camera instead of the PSPC. A triangular form electric field was used for the quasi-static measurement while step-form and square-form fields were used for the transient layer response measurement.

3. Results

The time-integrated X-ray diffraction profile from TK-C101 in the SmA phase was measured as a function of

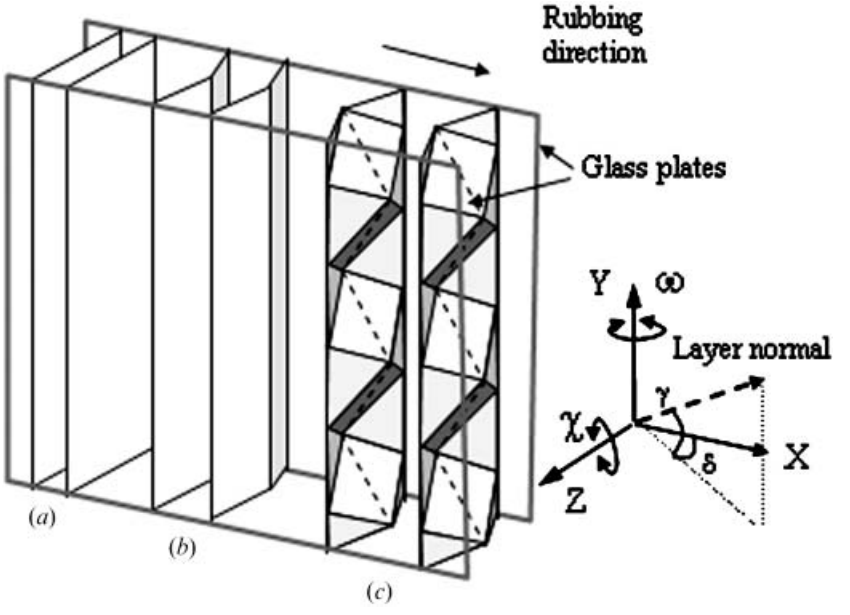

Figure 1. Schematic drawing of layer structure. (*a*) Bookshelf, (*b*) vertical chevron and (*c*) compound chevron (vertical and horizontal chevron) layer structures. Thin dotted lines are a guide to eye. Coordinates and rotation axes are also shown. X-rays are incident along Z.

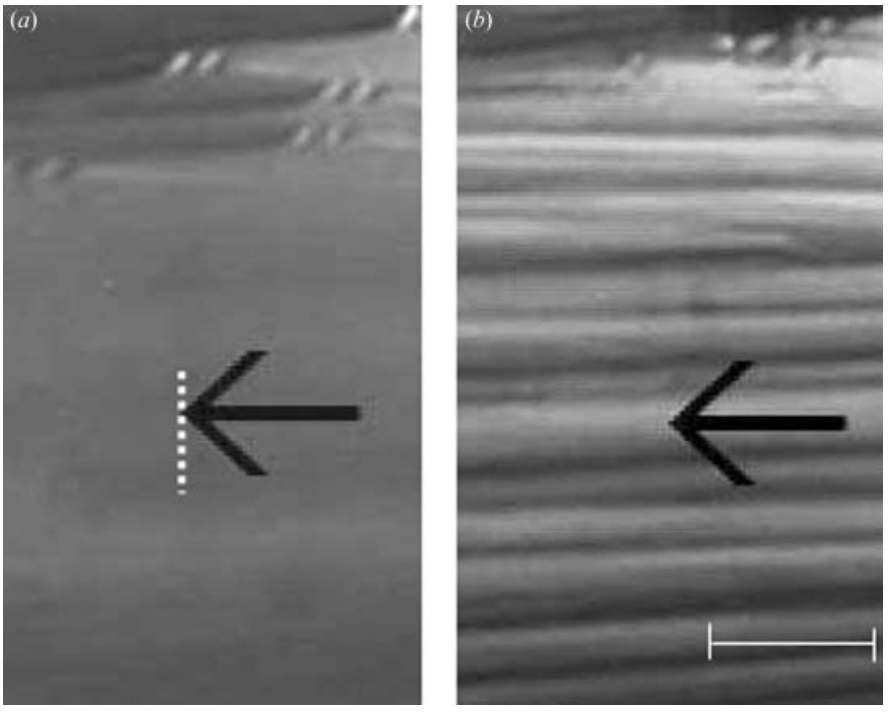

Figure 2. Polarizing optical micrographs of textures of the initial stage (*a*) before field application, (*b*) during ± 20 V triangular form electric field application. A scale mark is 50 μm. A white dotted line in (a) shows the region of the X-ray measurement (40 μm) shown in figure 3.

position. Before the field application, no conspicuous texture is observed in a polarizing optical micrograph, figure 2 (*a*). Figures 3 (*a*) and 3 (*b*) show series of ω- and χ-profiles, respectively, along the *Y*-direction, i.e. normal to the rubbing direction. The bookshelf structure (single peak at around $\omega=0^\circ$ and $\chi=0^\circ$) is seen in these figures.

When the triangular-form electric field (5 Hz) was applied to the sample, peaks in the ω-profile and χ-profile became broad. With greater than ± 10 V

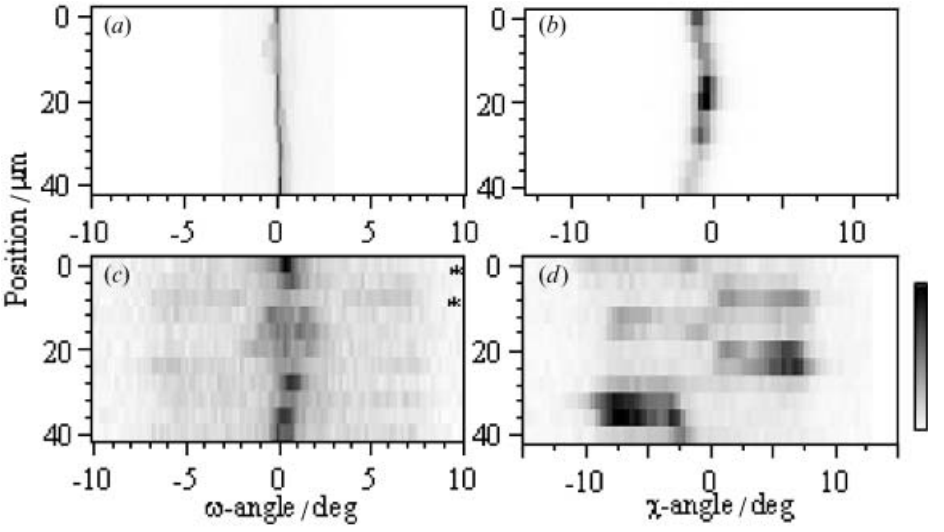

Figure 3. (*a*), (*c*) Series of ω-profiles, and (*b*), (*d*) series of χ-profiles, as a function of the vertical position (*Y*-direction). (*a*) and (*b*) are before the field application; (*c*) and (*d*) are during the application of a triangular field of ± 20 V. The χ-profiles were obtained at the peak near $\omega=0^\circ$. The scanning step in the *Y*-direction was 4 μm. Marks (*) in (*c*) indicate positions where the time-resolved profiles of figure 4 were obtained. The darker part corresponds to the higher diffracted intensity; X-ray intensities were normalized by the highest intensity in each figure.

application, a clear stripe texture develops over the entire field of view, its width broadening after a few hours of field application, figure 2 (*b*). At ± 20 V, a series of the ω-profiles, figure 3 (*c*), shows a central peak at $\omega=0^\circ$ together with broad and weak sub-peaks (or shoulder) around $\omega=\pm 6^\circ$, which change their intensities from position to position. The χ-intensity distribution, figure 3 (*d*), obtained at $\omega=0.4^\circ$ shows alternate intensity variation between the low and high angle peaks.

Figures 4 (*a*) and 4 (*c*) show the time-resolved MCS-mode ω-profiles for one cycle of the triangular wave-form (± 20 V). They are obtained from positions which correspond to the first and third lines in figure 3 (*c*), respectively, and are 8 µm apart. In both figures, two types of peak are observed: the stable central peak around $\omega=0^\circ$, and sub-peaks whose angular positions depend on the applied voltage. The maximum angular separation between sub-peaks at ± 20 V is about 15° in figure 4. The central peak in figure 4 (*a*) is much stronger than the sub-peaks, while that in figure 4 (*b*) is weak compared with the sub-peak, except for low field.

Corresponding time-resolved MCA-mode χ-profiles obtained at $\omega\sim 0^\circ$ show the double peak which depends on the applied field, see figures 4 (*b*) and 4 (*d*). At low field, the angle between two peaks is small, while it increases with increase in the applied field. The low angle peak is stronger than the high angle peak in figure 4 (*c*), while both peaks at high field have a similar intensity, though weak in figure 4 (*d*). These observations confirm that the h-chevron is dominant in figures 4 (*a*) and 4 (*b*), while the v-chevron is a main structure in figures 4 (*c*) and 4 (*d*). The layer deflection angles, i.e. chevron angles δ and γ, are determined to be 7–8° at the applied voltage of ± 20 V (~ 3 V µm^{-1}). The layer deflection angle increases linearly with the applied voltage, although saturation behaviour at high voltage

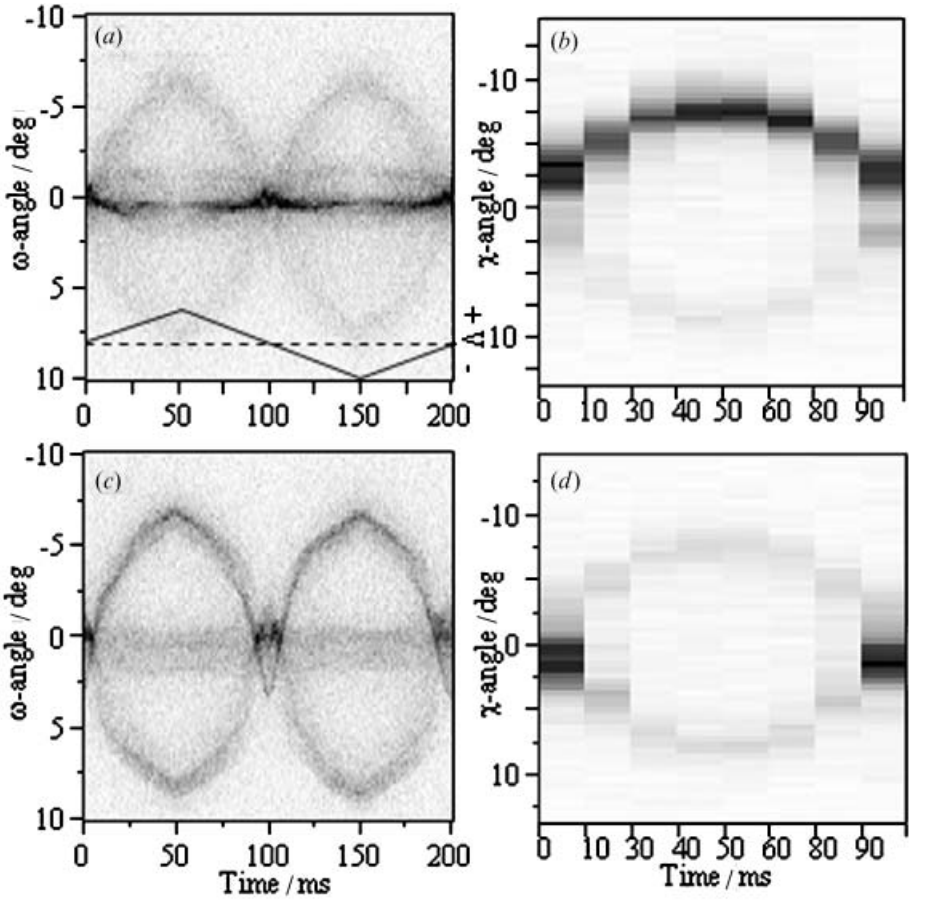

Figure 4. Time-resolved X-ray diffraction profiles. Upper figures (*a*) and (*c*), and lower figures (*b*) and (*d*), were obtained 8 µm apart along the *Y*-direction. (*a*) and (*c*) are time-resolved ω-profiles for one cycle of the triangular wave form (5 Hz). (*b*) and (*d*) are time-resolved χ-profiles for a half cycle of the wave-form. Note the sampling time (abscissa) of the χ-profile comprises unequal interval. The time resolutions were 0.2 and 10 ms for the ω-profiles and χ-profiles, respectively. A wave-form applied to the sample is schematically shown in (*a*); maximum applied voltage was ± 20 V.

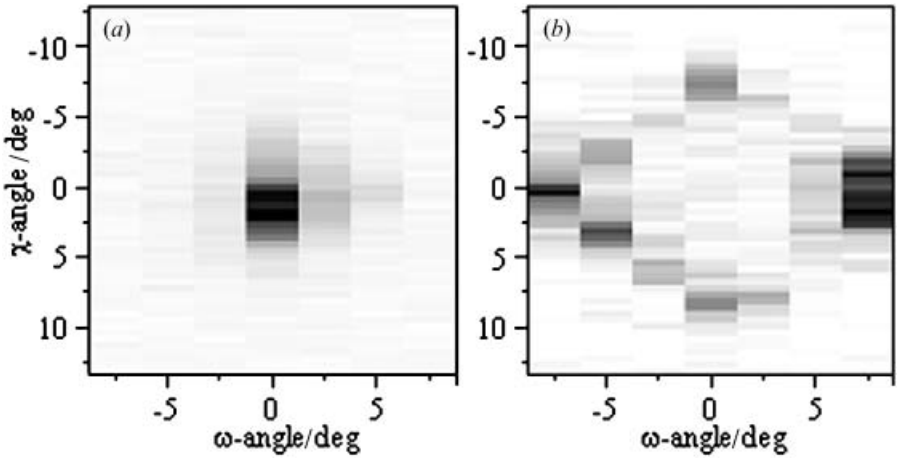

Figure 5. Time-resolved χ-profiles as a function of the ω-angle. (*a*) and (*b*) were obtained at 0–10 ms (0–4 V) and 40–50 ms (16–20 V), respectively, for a triangular wave form of 5 Hz. The analysing position was the same as that for figures 4 (*c*) and 4 (*d*).

is often observed. The relationship between ω- and χ-profiles is shown in figure 5, which is obtained from a series of time-resolved χ-profiles as a function of ω. At the low voltage, figure 5 (*a*), the single peak appears around $\omega=0^\circ$ and $\chi=0^\circ$ indicating the bookshelf structure, although the peak width, both in ω- and χ-angle, increases compared with the initial bookshelf structure, figures 3 (*a*) and 3 (*b*). At high voltage, figure 5 (*b*), the double peak at $\omega=0^\circ$ (h-chevron) and the single peak at $\omega=\pm 7^\circ$ (v-chevron) are realized simultaneously. It can also be seen in figure 5 (*b*) that an intermediate structure appears between the h-chevron and the v-chevron ($0^\circ<|\omega|<7^\circ$), i.e. the chevron layer gradually changes from one chevron to an other.

The time-integrated profiles of figure 6 are obtained from figure 4 and they characterize well two types of layer response. By comparing figure 6 with figure 3, the alternate appearance of v- and h-chevrons (the compound chevron structure) is clearly visible. This positional dependence was also confirmed from a series of time-resolved measurements similar to figure 4 as a function of position.

Figure 4 shows typical time-resolved microdiffraction profiles at medium to relatively high a.c. field observed in samples exhibiting stripe texture. When the region without stripe texture in the same sample is measured, the ω-profile shows no central peak even at high field, as shown in figure 7 (*a*), which definitely shows that the layer structure is v-chevron alone. In the region without stripe texture, no periodic change in the diffraction profile was observed.

Although most of the experiments were performed with a one-side rubbing cell, no systematic difference was observed in both-sides rubbing cells. On the other

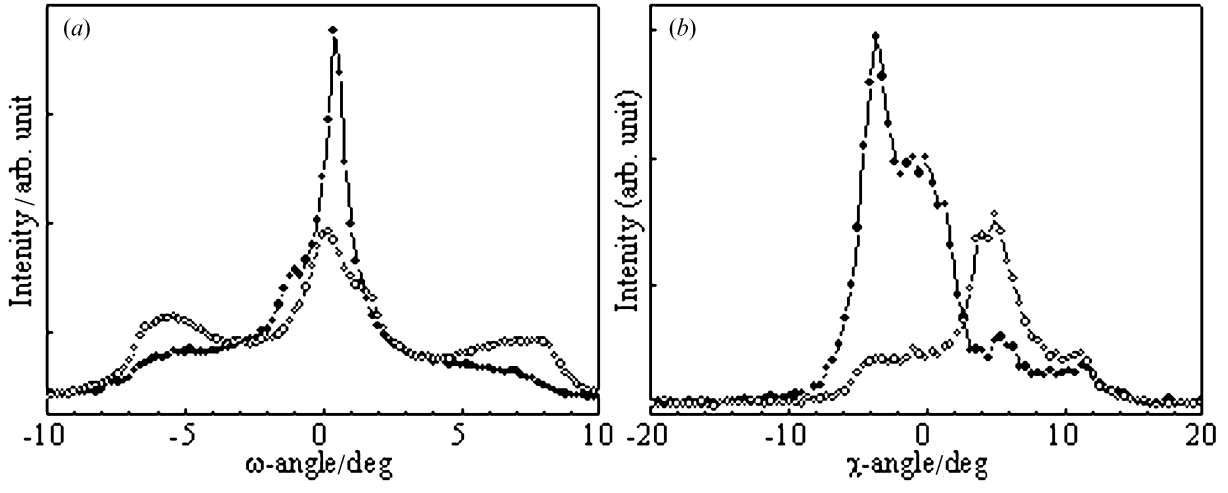

Figure 6. Time-integrated intensity obtained from figure 4 for (*a*) the ω- profile and (*b*) the χ-profile. Closed and open circles correspond to different positions, namely figures 4 (*a*) and 4 (*b*) and figures 4 (*c*) and 4 (*d*), respectively.

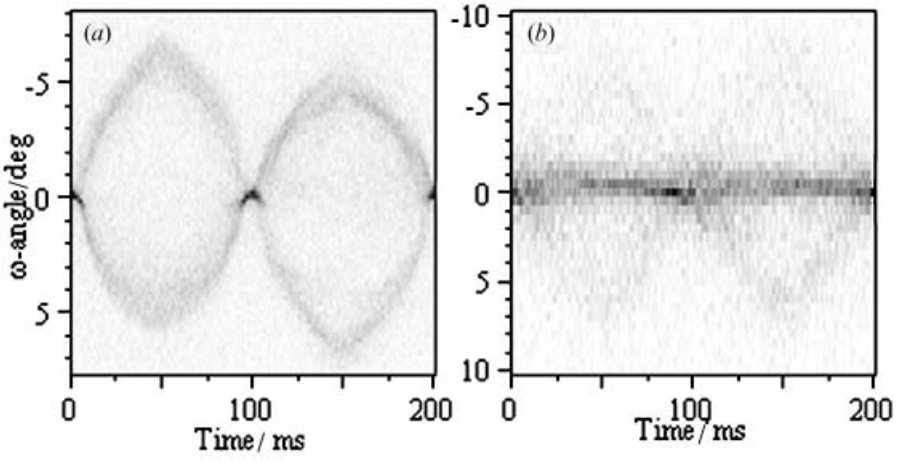

Figure 7. Time-resolved ω-profiles for one cycle of triangular wave-form (5 Hz). (*a*) was obtained from the region without stripe (± 20 V). (*b*) was obtained from the stripe region for ± 40 V application.

hand, many small grains appeared in the cell with no rubbing treatment. When the horizontally aligned small region was analysed in such a cell, sharp peaks appeared in the time-resolved ω-profile, and the χ-profile again showed the double peak at high field, similar to figure 4. The v-chevron or tilted bookshelf structure in combination with the h-chevron was developed locally, even without rubbing. No periodicity could be confirmed in these cells with no rubbing treatment.

Up to the maximum applied field in the present study, namely 40 V ($\sim 6.7\,\mathrm{V\,\mu m^{-1}}$), the typical profile was more or less similar to figure 4. As the applied field increased, however, the relative intensity of the central peak (h-chevron) in the ω-profile became stronger as seen in figure 7 (*b*). After the field was turned off, two types of layer structure were realized: one was a bookshelf structure in which the fwhm of the diffraction peak was slightly broader than the initial one; the other was a compound chevron structure similar to that under high electric field, with reduced chevron angle, figures 3 (*c*) and 3(*d*). In the former, there was no conspicuous texture in an optical micrograph while the stripe texture was still discernible in the latter.

Even for a low applied field, the layer response was roughly similar to that for the higher applied field; the v-chevron was realized and the h-chevron component appeared when the stripe texture developed. Figures 8 (*a*) and 8 (*b*) show the time-resolved ω-profile for 2.5 and 5 V application, respectively. The maximum chevron angle deduced from the angular separation of the sub-peaks depends on the applied field. It is noted that the layer responds to the applied field above the threshold. A similar threshold behaviour is observed at the higher applied voltage in figures 4 (*a*) and 4 (*c*). The threshold voltage was usually 1–2 V (about $0.3\,\mathrm{V\,\mu m^{-1}}$), but varied from 0 V (no threshold) to 5 V depending on the sample. Whereas the *in situ* measurement of the optical response showed a linear response to the applied field in accordance with the previous experiments [6], threshold response in the electroclinic effect was observed for the first time. At low field, the layer shrinkage due to molecular tilt ($\sim 1^\circ$) is so small that the simple layer shrinkage is favorably compared to chevron formation, resulting in an apparent threshold behaviour. The diffraction profile at low field, however, seems to depend strongly on the sample. At low voltage, the contribution to layer formation from the interface is relatively large; the early stage of chevron formation is affected by the alignment condition, which depends on the sample and sample history.

The change in layer spacing during the field application was measured using the II CCD camera. Although the layer spacing measurement is usually made by ω-2θ scanning, the present experiment adopted the observation of the diffraction image on the CCD camera with a fixed ω angle. The layer spacing as a function of applied field, obtained by a time-resolved technique for a triangular field, is shown in the table. Also shown is the layer spacing deduced from the chevron angle: $\Delta d/d \sim (\delta \text{ or } \gamma)^2/2$. The layer spacing changes during the field application and correlates well with the chevron angle, i.e. the chevron structure formation is due to the layer constriction.

Using a step wave-form electric field (100 Hz, ± 20 V), the transient layer response at the rising edge (0 V to high voltage) and the falling edge (high voltage to 0 V) were measured. The profile changes from single peak to double peak for the ω-profile at the rising edge, figure 9 (*a*), and from double peak to single peak at the falling edge, figure 9 (*b*). It is noted that at this

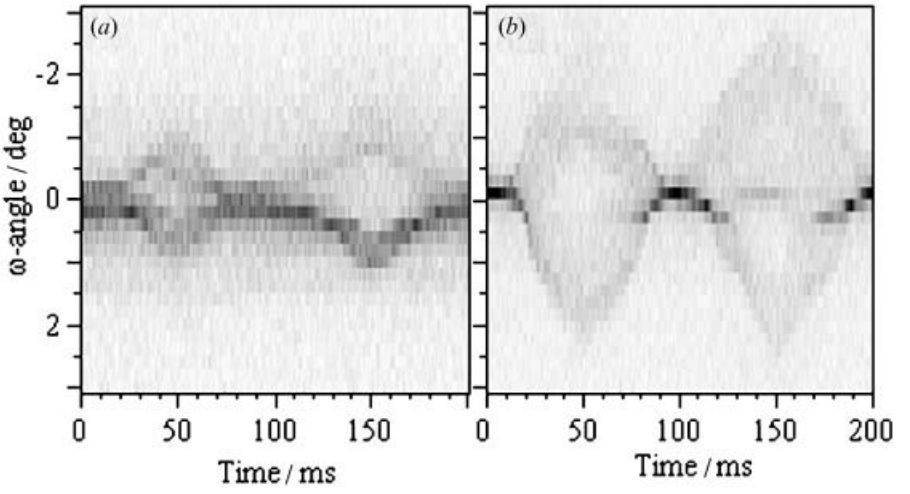

Figure 8. Time-resolved ω-profiles for one cycle of the triangular wave-form (5 Hz). (*a*) and (*b*) were obtained for 2.5 and 5 V, respectively. The cell gap was 7 µm.

analysing position, the central peak at the high voltage is very weak, i.e. the v-chevron is a dominant structure. The major change in profile is complete less than 15 and 10 µs for the rising and falling edges, respectively, followed by a slow relaxation of more than 20 µs. The time-resolved χ-profiles in figures 9 (*c*) and 9 (*d*) show a similar response time. The electro-optical response measured simultaneously by X-ray diffraction was around 10 µs, although the measurement area (about 100 µm in diameter) was much larger than the X-ray microbeam size. The exponential response obtained can be interpreted qualitatively as the system having a constant viscosity. The faster response time at the falling edge than that at the rising edge suggests a relatively strong anchoring force.

The transient response to the polarity inversion (positive to negative voltage and *vice versa*) is shown in figure 10. Both ω- and χ-profiles show that the layer starts to relax into the low field structure within 5 µs, and returns to the high field structure gradually during about 30 µs. The optical response is quite similar to the layer response, as shown in figure 10 (*a*). Compared with figure 9, the response at the polarity inversion is the superposition of the responses at the falling and the rising edges. From these transient response measurements, the response under 5 Hz triangular wave-form can be regarded as static, except thtat the response itself depends on the maximum applied field.

4. Discussion

We first discuss the development of the compound chevron structure. In the electroclinic effect, molecules tilt in the plane normal to the applied electric field, resulting in layer shrinkage. In order to release the induced strain, the h-chevron is the proper layer structure, since it can accomplish in-plane molecular rotation. Because of the anchoring effect, however, it is difficult to realize h-chevrons at the substrate interface under a weak electric field. It is well known that the v-chevron structure is formed in the SmC* phase due to layer shrinkage with decreasing temperature, with molecules fixed at the substrate interface [7, 28]. For the same reason, the v-chevron is formed at the initial stage of the electroclinic effect, although layer shrinkage in the electroclinic effect has a different origin from that causing v-chevron formation in the SmC* phase. In order to generate h-chevrons in the homogeneous v-chevron structure, a needle-defect is formed, similar to

Table. Layer spacing as a function of applied voltage of triangular wave-form (5 Hz, $\pm$20 V). Time resolution was 12.5 ms. d_0 is the layer spacing obtained during 0–5 V application.

Time/ms	Applied voltage/V	ω-angle/deg	$\Delta d/d_0$/% from $\Delta\theta/\theta$	$\Delta d/d_0$/% from δ or γ
12.5–25	5–10	0	−0.18 $\pm$0.02	−0.2
25–37.5	10–15	0	−0.33	−0.33
37.5–50	15–20	0	−0.43	−0.46
37.5–50	15–20	5	−0.48	−0.47

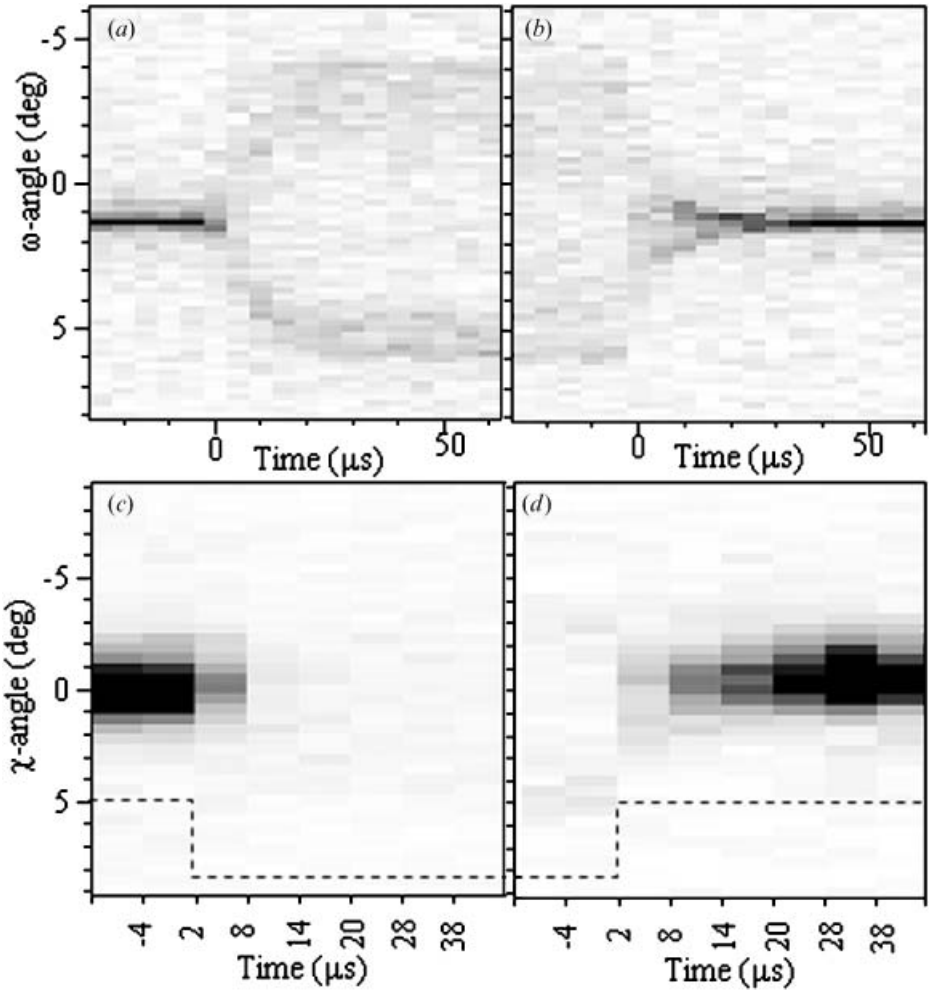

Figure 9. Time-resolved ω-profiles, (*a*)and (*b*), and χ-profiles, (*c*) and (*d*), for the step wave-form (100 Hz, $\pm$20 V). (*a*) and (*c*) were obtained for the rising edge (0 to 10 V) and (*b*) and (*d*) for the falling edge (10 to 0 V). The zero of the time scale is taken at the time of the field change. χ-profiles were obtained at ω=1°. The time resolutions were 1 and 5 μs for ω-profiles and χ-profiles, respectively. Dotted lines show the applied voltage schematically.

the layer transformation in SmC* and SmC_A* phase under an electric field [6, 26, 27, 29]. With the needle-defect, h-chevron structure in the bulk can be partly realized without rearrangement of surface molecules. The formation and development of the needle-defect corresponds with the appearance of the so-called stripe texture under the polarizing microscope. When the needle-defect covers the whole area, the compound chevron structure is formed, in which the h-chevron and the v-chevron appear alternately along the layer. With increasing electric field, the h-chevron, which is more favoured than the v-chevron in the electroclinic effect, becomes dominant, so that the layer and molecules at the surface rearrange against the anchoring force. Naturally, if no needle-defect is generated due to the lack of the appropriate nucleation centre, the v-chevron is a dominant layer structure in even medium to high fields, see figure 7 (*a*). These results are different from previous experiments in which the h-chevron layer structure was dominant [12–14], while the importance of the anchoring effect of the surface stabilized cell in chevron layer formation is clearly demonstrated in the present experiment.

From experimental results together with these considerations, the layer structure at medium electric field can be depicted as shown in figure 1. The layer structure at the initial stage and at 0 V during the a.c. cycle is a bookshelf structure, see figure 1 (*a*), as deduced from figures 3 (*a*) and 3 (*b*). Figure 1 (*b*) shows the pure v-chevron and corresponds to figure 7 (*a*), while the compound chevron structure associated with the stripe texture (figure 4) is shown in figure 1 (*c*). The layer structure is based on the assumption that at the alignment interface the layer is difficult to transform

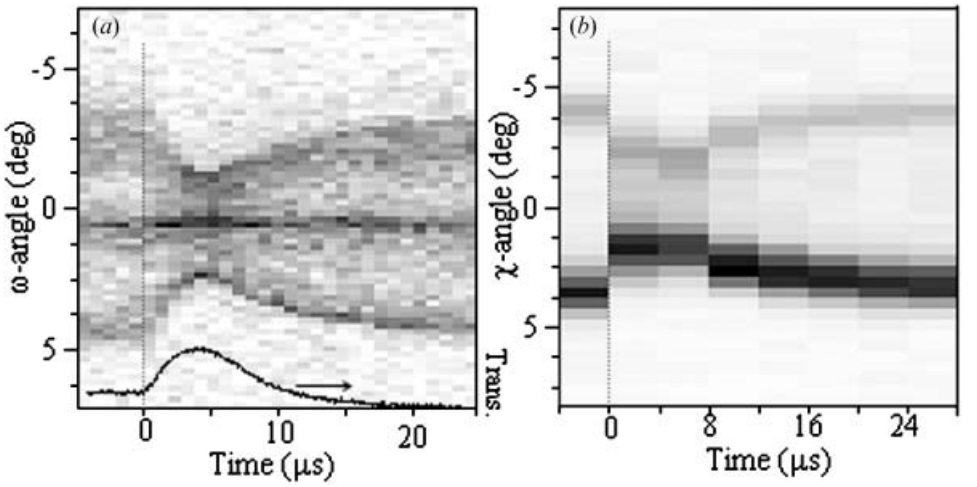

Figure 10. Time-resolved ω-profiles (*a*) and χ-profiles (*b*) for the square wave-form (1 kHz, ± 10 V). The solid line in the lower part of (*a*) shows the change in optical transmittance. The time resolutions were 1 and 3 μs for ω-profiles and χ-profiles, respectively.

during one cycle of the a.c. field. At higher field, however, rearrangement at the interface actually occurs. The compound chevron structure is quite similar to the layer structure of the SmC* and SmC_A* phases under high field [26, 27]. The characteristic of the layer structure in the present electroclinic effect is that the v-chevron is always clearly observed. For SmC* and SmC_A* phases, the initial layer structure is the v-chevron with a large chevron angle (typically around 20°); it then approaches the bookshelf structure by way of the compound chevron structure. When the bookshelf structure is partly realized in these materials, the change in surface alignment is considerable. In the electroclinic effect, by contrast, the initial layer is in the bookshelf structure and the chevron angle under the applied field is small (less than 10° in the present experiment), so the surface alignment is not seriously affected. Considering the δ-γ dependence in figure 5, however, the structure of figure 1 (*c*) is somewhat modified and the layer continuously changes its curvature from v-chevron to h-chevron. The relation $\cos\theta/\cos\delta\cos\gamma$=const. [7, 30], which is deduced from the SmC* layer tilt (θ is the molecular tilt angle), seems to be applicable also to this case.

The stripe texture corresponds closely to the h-chevron structure. The stripe width approximates to the cell thickness when first generated [6, 7], and it often widened after the application of the electric field for several hours. The stripe texture was sometimes observed even after the field was switched off, and the corresponding diffraction profile showed that the chevron structure still remained. When the applied field is strong and/or the field is applied for a long time, the h-chevron part (initial lozenge shape) extends to the surface, and a portion of the surface molecules rearrange. The width of the stripe is no longer limited by the cell thickness and can be extended. At the same time, the stripe texture becomes stable due to the molecular rearrangement, and remains even after the electric field is turned off. A similar behaviour of surface molecules has been seen in the SmC* phase under a high electric field [26].

During this experiment, the layer response sometimes seemed to depend on the polarity of the applied field, such as seen in figure 7 (*a*) and figures 8 (*a*) and 8 (*b*), while most of the experimental results seemed to be independent of the field polarity. The asymmetric or anti-symmetric response in the profile cannot be discussed in detail at present due to the lack of information on the sense of the v-chevron and the depth profile. For example, the asymmetric response might arise from a change in direction of the v-chevron sense or in the ratio of the branches of the asymmetric v-chevron. The present phenomenon, together with the previous observation in the SmC_A* phase [25], might be related to the microscopic process of layer rotation under an asymmetric electric field [31, 32].

5. Summary

The layer structure in the electroclinic effect was analysed by time-resolved synchrotron X-ray microdiffraction. Under a medium applied field, not only horizontal chevrons but also vertical chevrons appeared alternately along the layer. With increasing field, the horizontal layer became a dominant structure while the vertical chevrons still remained. The stripe texture corresponded to the horizontal chevron. At high field

or by prolonged application of a relatively high field, surface molecules rearranged resulting in deterioration of the alignment at the interface. The transient layer response was very close to the optical response.

In the present experiment, the layer structure alone has been observed and discussed. In order to analyse the layer response fully, the change in molecular orientation in the layer is quite important. The layer structure is so complicated that the corresponding molecular orientation is informative for discussion of molecular ordering in the electroclinic effect. Time-resolved high angle X-ray scattering experiments are now under way to clarify the molecular response.

Acknowledgements

The authors would like to thank the staff of the Photon Factory for their help during experiments. This work was carried out under the approval of the Photon Factory Advisory Committee (Proposal No. 00G279 and 02G293); it was partly supported by Grant-In-Aid for Scientific Research on Priority Area (B) (12129202 and 12129206), the Ministry of Education, Science, Sports and Culture, Japan.

References

[1] S. Garoff, R.B. Meyer. *Phys. Rev. Lett.*, **38**, 848 (1977).
[2] S.T. Lagerwall. *Ferroelectric and Antiferroelectric Liquid Crystals*. Wiley, Weinheim (1999).
[3] P.A. Williams, N.A. Clark, M.B. Ros, D.M. Walba, M.D. Wand. *Ferroelectrics*, **121**, 143 (1991).
[4] S.D. Lee, J.S. Patel. *Phys. Lett. A*, **155**, 435 (1991).
[5] J. Pavel, M. Glogarova. *Liq. Cryst.*, **9**, 87 (1991).
[6] R.F. Shao, P.C. Williams, N.A. Clark. *Ferroelectrics*, **121**, 127 (1991).
[7] T.P. Rieker, N.A. Clark, G.S.S. Smith, D.S. Parmar, E.B. Sirota, C.R. Safinya. *Phys. Rev. Lett.*, **59**, 2658 (1987).
[8] M. Johno, Y. Ouchi, H. Takezoe, A. Fukuda, K. Terashima, K. Furukawa. *Jpn. J. appl. Phys.*, **29**, L111 (1990).
[9] J. Fünfschilling, M. Schadt. *Jpn. J. appl. Phys.*, **30**, 741 (1991).
[10] M. Johno, A.D.L. Chandani, Y. Takanishi, Y. Ouchi, H. Takezoe, A. Fukuda. *Ferroelectrics*, **114**, 123 (1991).
[11] H. Okada, M. Shibata, H. Onnagawa. *Jpn. J. appl. Phys.*, **35**, 5426 (1996).
[12] G.P. Crawford, R.E. Geer, J. Naciri, R. Shashidhar, B.R. Ratna. *Appl. Phys. Lett.*, **65**, 2937 (1994).
[13] A.G. Rappaport, P.A. Williams, B.N. Thomas, N.A. Clark, M.B. Ros, D.M. Walba. *Appl. Phys. Lett.*, **67**, 362 (1995).
[14] R.E. Geer, S.J. Singer, J.V. Selinger, B.R. Ratna, R. Shashidhar. *Phys. Rev. E*, **57**, 3059 (1998).
[15] K. Skarp, G. Anderson, T. Hirai, A. Yoshizawa, K. Hiraoka, H. Takezoe, A. Fukuda. *Jpn. J. appl. Phys.*, **31**, 1409 (1992).
[16] F. Giesselmann, P. Zugenmaier. *Phys. Rev., E*, **52**, 1762 (1995).
[17] J.V. Selinger, J. Xu, R.L.B. Selinger, B.R. Ratna, R. Shashidhar. *Phys. Rev., E*, **62**, 666 (2000).
[18] A. Tang, S. Sprunt. *Phys. Rev., E*, **57**, 3050 (1998).
[19] S.M. Said, S.M. Beldon, S.J. Elston. *Ferroelectrics*, **277**, 141 (2002).
[20] F.J. Bartoli, J.R. Lindle, S.R. Flom, R. Shashidhar, G. Rubin, J.V. Selinger, B.R. Ratna. *Phys. Rev. E*, **58**, 5990 (1998).
[21] P. Cluzeau, P. Barois, H.T. Nguyen, C. Destrade. *Eur. Phys. J.*, **B 3**, 73 (1998).
[22] P. Cluzeau, P. Barois, H.T. Nguyen. *Eur. Phys. J.*, **E 7**, 23 (2002).
[23] L.S. Matkin, H.F. Gleeson, L.J. Baylils, S.J. Watson, N. Bowring, A. Seed, M. Hird, J.W. Goodby. *Appl. Phys. Lett.*, **77**, 340 (2000).
[24] S.J. Watson, L.S. Matkin, L.J. Baylis, N. Bowring, H.F. Gleeson, M. Hird, J. Goodby. *Phys. Rev., E*, **65**, 31705 (2002).
[25] Y. Takahashi, A. Iida, Y. Takanishi, T. Ogasawara, K. Ishikawa, H. Takezoe. *Jpn. J. appl. Phys.*, **40**, 3294 (2000).
[26] Y. Takahashi, A. Iida, Y. Takanishi, T. Ogasawara, M. Nakata, K. Ishikawa, H. Takezoe. *Phys. Rev., E*, **67**, 051706 (2003).
[27] Y. Takanishi, A. Iida, K. Ishikawa, H. Takezoe, A. Fukuda. *Jpn. J. appl. Phys.*, **35**, 683 (1996).
[28] Y. Ouchi, H. Takano, H. Takezoe, A. Fukuda. *Jpn. J. appl. Phys.*, **27**, 1 (1988).
[29] A. Iida, T. Noma, H. Miyata. *Jpn. J. appl. Phys.*, **35**, 160 (1996).
[30] K. Takada, T. Noma, T. Togano, T. Mukaide, A. Iida. *Jpn. J. appl. Phys.*, **42**, 4431 (2003).
[31] M. Ozaki, H. Moritake, K. Nakayama, K. Yoshino. *Jpn. J. appl. Phys.*, **33**, L1620 (1994).
[32] I. Dierking, B. Glusen, S.T. Lagerwall, C.K. Ober. *Phys.Rev., E*, **61**, 1593 (2000).